Available online at www.sciencedirect.com
ScienceDirect
Geochimica et Cosmochimica Acta 71 (2007) 186–201
Geochimica
www.elsevier.com/locate/gca

Quartz solubility in the two-phase and critical region of the NaCl–KCl–H_2O system: Implications for submarine hydrothermal vent systems at 9°50′N East Pacific Rise

D.I. Foustoukos *, W.E. Seyfried Jr.

Department of Geology and Geophysics, University of Minnesota, Minneapolis, MN 55455, USA

Received 14 March 2006; accepted in revised form 29 August 2006

Abstract

Experiments were performed to investigate quartz solubility in Cl-bearing aqueous solutions at temperature (365–430 °C) and pressure conditions (219–381 bars) near and within the two-phase region of the NaCl–KCl–H_2O system. Dissolved SiO_2 concentrations increased with pressure along a given isotherm, although the magnitude of this decreased with increasing proximity to the two-phase boundary. Upon intersection of the two-phase boundary, however, significant concentrations of dissolved SiO_2 characterized vapor-rich fluids at both subcritical and supercritical conditions. For these fluids, dissolved silica concentrations ranged from 2.81 to 14.6 mmolal, increasing with dissolved chloride concentration. The experimental data permit regression of a density-based relationship, taking account of non-ideal activity–concentration effects, which can be used to better constrain temperatures and pressures from dissolved SiO_2 and chloride in high temperature vent fluids at mid-ocean ridges. Accordingly, pressure and temperature conditions in subseafloor hydrothermal reaction zones at 9°50′N East Pacific Rise (EPR) were estimated applying data from this experimental study to interval (1991–2002) and new field data (2004). Results indicate reaction zone at conditions ranging from 420 to 430 °C at 600 to 1500 m below seafloor. Thus, conditions predicted for 9°50′N East Pacific Rise (EPR) vent fluids suggest that supercritical phase separation might be more common than previously thought.

1. Introduction

Dissolved silica exists as a component in all crustal fluids owing to the ubiquitous presence of quartz and other silica-rich minerals in coexisting lithologies. Thus, constraints imposed by quartz solubility have often been used to estimate temperature or pressure from dissolved SiO_2 concentrations in aqueous fluids (Mosebach, 1957; Jasmund, 1958; Wasserburg, 1958; Wasserburg and Wood, 1958; Wood, 1958; Walther and Helgeson, 1977; Fournier, 1983; Fournier and Potter, 1983; Von Damm et al., 1991). Applying quartz solubility constraints to submarine hydrothermal systems, however, requires knowledge of the effects of dissolved chloride on quartz–fluid equilibria (Khitarov, 1956; Kitahara, 1960; Anderson and Burnham, 1967; Ganeyev, 1975; Hemley et al., 1980; Fournier et al., 1982; Fournier, 1983; Saccocia and Seyfried, 1990; Von Damm et al., 1991; Xie and Walther, 1993; Newton and Manning, 2000; Shmulovich et al., 2001). Accordingly, semi-empirical equations depicting quartz solubility have been developed for NaCl-bearing fluids (Fournier, 1983; Von Damm et al., 1991). These algorithms are based on experimental studies at a broad range of P–T conditions, although data are limited in the critical region of seawater and NaCl equivalent systems (~3.2 wt% NaCl). Thus, uncertainties can be introduced when these relations are used to predict temperature and pressure from dissolved SiO_2 for this particular region in P–T space, especially when dissolved chloride changes with temperature and pressure, as is often the case in the critical region of NaCl–H_2O system.

* Corresponding author. Fax: +1 202 478 8901.
E-mail address: dfoustoukos@ciw.edu (D.I. Foustoukos).

0016-7037/$ - see front matter © 2006 Elsevier Inc. All rights reserved.
doi:10.1016/j.gca.2006.08.038

Evidence indicates critical phenomena in subseafloor reaction zones of many hydrothermal systems. For example, vent fluids at 9–10°N East Pacific Rise (EPR) have relatively high measured temperatures and contain dissolved Cl concentrations that depart significantly from seawater values (Von Damm, 2000; Von Damm, 2004), suggesting near-critical conditions at times in the temporal evolution of the system (Von Damm et al., 1995; Oosting and Von Damm, 1996; Von Damm et al., 1997; Von Damm, 2004). Phase separation effects have also been reported for vent fluids at the Main Endeavour Field, Juan de Fuca Ridge (Butterfield et al., 1994; Seyfried et al., 2003).

To address the need to augment quartz solubility data in the critical region of seawater, hydrothermal experiments involving quartz–fluid equilibria were performed. Experiments were conducted at temperatures and pressures from 365 to 430 °C and 219 to 381 bars, respectively, while dissolved chloride concentrations ranged from 0.015 to 1.135 molal. Dissolved SiO_2 concentrations were explicitly determined in the bulk fluid prior to phase separation and in the vapor fraction upon intersection of the two-phase boundary for both subcritical and supercritical conditions. In addition to quartz, K–feldspar and muscovite were utilized with dissolved K concentrations buffering $pH_{(T,P)}$[1] at slightly acidic values, generally consistent with the pH of subseafloor hydrothermal vent fluids (Ding and Seyfried, 1992).

In addition to experimental data, we also report dissolved SiO_2 concentrations of selected vent fluids at 9°50′N EPR sampled in February 2004. These data, together with previous measurements of dissolved chloride, SiO_2 and temperature for the same vent fluids, initially sampled in 1991–1992 following volcanic eruptions (Haymon et al., 1993; Rubin et al., 1994; Von Damm, 2000; Von Damm, 2004), provide a robust dataset and allow development of a more complete understanding of the role of temperature, pressure and dissolved chloride on quartz solubility effects in subseafloor reaction zones at 9°50′N East Pacific Rise.

2. Methods

2.1. Experimental procedures and design

Hydrothermal experiments were performed using a flexible gold reaction cell, which allows time series sampling of internally filtered fluid at experimental conditions (Seyfried et al., 1987). Mineral reactants used for the experiments (quartz, K–feldspar, and muscovite) were obtained from Wards Natural Science Establishment or from mineral collections at the University of Minnesota. All minerals were sieved to collect the 325–200 mesh size fraction (44–74 μm), which then was analyzed by XRD, SEM, and ICP-MS to assure chemical and mineralogical purity (Table 1). The composition of the starting fluid was 0.32 molal NaCl and 0.25 molal KCl yielding 0.57 molal total dissolved Cl. A fluid of this composition coexisting with K–feldspar–muscovite–quartz, buffers $pH_{(T,P)}$[2] at approximately 5 for the range of conditions (T, P, x) investigated. In addition to experiments involving K–feldspar and quartz in KCl and NaCl aqueous solutions, a "control experiment" with only quartz and NaCl fluid having ionic strength similar to the compositionally more complex systems was also performed. The control experiment was needed to establish whether or not Na and K affected quartz solubility differently. Prior to initialization of the experiments, starting fluid was acidified (pH 3.5) to avoid mineral precipitation during the heat up stage.

Table 1
Composition of mineral reactants used in hydrothermal experiments

Wt%	Quartz	K–feldspar	Muscovite
SiO_2	99.8	64.2	45.1
Al_2O_3	0.03	18.2	29.3
FeO*	0.04	0.55	4.38
MgO	0.02	0.12	0.97
CaO	0.50	1.38	0.31
Na_2O	0.03	2.62	0.56
K_2O	0.07	11.8	9.93
Total	100.5	98.9	90.6

Quartz, SiO_2.
K–feldspar, $(K_{0.7}Na_{0.2}Ca_{0.1})AlSi_3O_8$.
Muscovite, $(K_{1.8}Na_{0.16}Ca_{0.04})(Al_{3.3}Fe_{0.5}Mg_{0.2})(Si_{6.4}Al_{1.6}O_{20})(OH_4)$.
* $FeO = Fe_2O_3 + FeO$.

The experiments were conducted at conditions near the critical point and in the two-phase region of the seawater-like starting fluid (Fig. 1). Temperature and pressure conditions that intercept the two-phase boundary, however, result in the formation of vapors and brines, which when sampled change the bulk composition of the system. As a consequence of this, we actually examined quartz solubility effects for a range of dissolved chloride concentrations (0.015–1.135 molal Cl) (Tables 2–4).

Phase separation was typically induced by decreasing pressure (Fig. 1). Although samples of conjugate brine and vapor could be obtained by changing the orientation of the reaction vessel (Berndt et al., 1996), the relatively small volume (<40 ml) of the reaction cell and the seawater-like chlorinity of the starting fluid precluded formation of significant amounts of brine at most conditions. Accordingly, brine samples were not taken during the present study. Changes in pressure and temperature during sampling were insignificant due to the large volume of water that filled the autoclave (750 ml) surrounding the reaction cell (Seyfried et al., 1987), and the small amount of fluid sample removed (~1.5 ml). Pressure was measured with a high precision Heise pressure gauge (CM-4709), while temperature was controlled using a proportioning controller

[1] $pH_{(T,P)}$ refers to the aH^+ estimated based on distribution of aqueous species at elevated temperatures and pressures.

[2] Estimated based on distribution of ionic species and the mineral-buffered aK^+/aH^+ ratios (Seyfried and Ding, 1993).

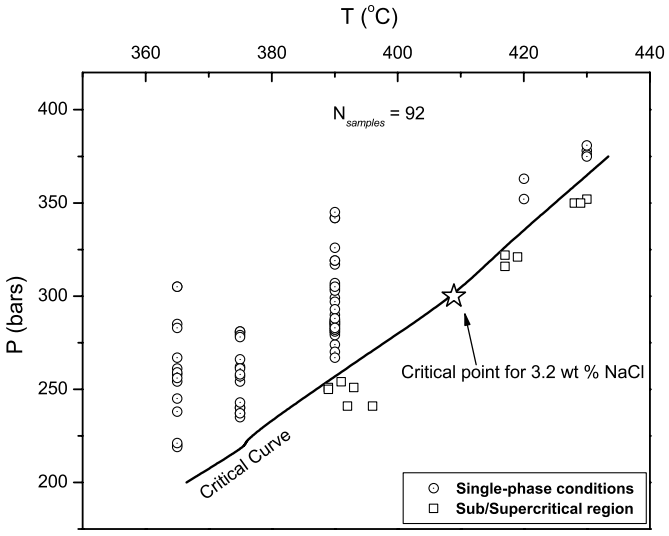

Fig. 1. Pressure–temperature diagram depicting experimental conditions used for the present study. A total of 92 fluid samples were collected, with 13 of those representing vapor endmembers of subcritical and supercritical phase separated Cl-bearing aqueous solutions. Phase relationships of the NaCl–H_2O system were determined from data and equations described by Berndt et al. (2001).

and measured using thermocouples inserted directly into the pressurized fluid (water). Each thermocouple was calibrated in place by measuring the temperature of steam-saturated water at 300–360 °C. The maximum uncertainty associated with reported temperatures was estimated to be ±1 °C. Uncertainties in the pressure gauge were determined by calibration against the Heise ST-2H Digital Pressure Indicator (±1 bar). For the bulk chlorinity investigated, temperature, pressure, and vapor composition (Table 4) are in excellent agreement with experimental and theoretical data for the NaCl–H_2O system (Bischoff, 1991; Berndt et al., 2001), providing an additional constraint on the accuracy of the temperature and pressure measurements during the experiments.

During the present study, equilibrium conditions were determined by reversing solubility from both undersaturation and supersaturation by systematically adjusting temperature and/or pressure. Moreover, theoretical modeling of quartz dissolution kinetics (Dove and Crerar, 1990; Dove, 1999) in a NaCl–KCl-bearing aqueous solution, indicated that the time intervals between fluid samples were more than sufficient for quartz–fluid equilibria to be achieved at all conditions investigated.

Fluid samples were analyzed for major and minor dissolved species relevant to the experimental system. In general, the first 0.2 ml of fluid removed from the reaction cell served to flush the sampling line and was discarded. Subsequent fluid samples were collected in glass gas-tight syringes. The first sample aliquot (0.5 ml) was used to measure dissolved Cl and $pH_{(25\ °C)}$, while additional aliquots were taken in separate syringes for determination of dissolved SiO_2 and all other dissolved species of interest. These samples were taken directly into 1 ml of 1 N HCl and immediately diluted 20-fold with distilled/deionized water to prevent mineral precipitation, in a manner consistent with procedures outlined by Von Damm et al. (1991).

Fluid samples were analyzed for Si, Na, and K by ICP-MS, while Cl was determined by ion-chromatography. Uncertainties in the dissolved concentrations of major elements are estimated to be approximately 2% of reported values at the 95% confidence interval. Molality units (e.g., mol/kg water: *molal*) were applied for mineral solubility data in keeping with the standard state convention for thermodynamic data in aqueous fluids. For hydrothermal vent fluid composition, however, mol/kg_{sol} units (formality) were adopted to be consistent with the concentration unit of choice used in the oceanographic community (Campbell et al., 1988).

2.2. Theoretical approach

Activity coefficients for charged aqueous species were calculated using the extended Davies model (Davies, 1962), as follows:

$$\log \gamma_i = -A_\gamma z_i^2 \left(\frac{\sqrt{I}}{1+\sqrt{I}} - 0.2I \right), \tag{1}$$

where z is the ionic charge and A_γ is the Debye–Huckle parameter taken to be equal to that of pure water at the temperatures and pressures of the experiments. The term "I" is the true ionic strength, which takes account of the distribution of aqueous species (c_i):

$$I = 0.5 \sum_i z_i^2 c_i \tag{2}$$

Activity coefficients, together with measured concentrations (m_i) of dissolved species, were used to calculate activities (a_i) of aqueous species, as follows:

$$a_i = m_i \gamma_i \tag{3}$$

For neutral species (e.g., $NaCl_{(aq)}$), activity coefficients were calculated from the Setchenow equation:

$$\log \gamma_i = b_i I \tag{4}$$

where b_i is a temperature and pressure dependent coefficient characteristic of the interaction between ith neutral species and the dominant component of the aqueous fluid. In the absence of data for b_i, however, a value of unity was assumed (see below).

Dissociation constant data for $NaCl_{(aq)}$, $KCl_{(aq)}$, $NaOH_{(aq)}$, $KOH_{(aq)}$, and $HCl_{(aq)}$ aqueous species were taken from Ho et al. (1994, 2000a,b, 2001), since these data are based on experimental measurements at conditions similar to the present study. Mineral hydrolysis data are from SUPCRT92 (Johnson et al., 1992) and the 1998 database update (Shock et al., 1997; Sverjensky et al., 1997). Thermodynamic properties of H_2O were calculated from the Sengers et al. (1983) and Haar et al. (1984) equations of state, as described by Johnson et al. (1992). In the two-phase region of the NaCl–H_2O system, the PVTx liquid–

Table 2
Chemical composition of fluid samples from quartz solubility experiments at near-critical conditions in the NaCl–KCl–H_2O system

Sample No.	Reaction time (h)	T (°C)	P (bars)	$SiO_{2(aq)}$ (mmolal)	Cl (mmolal)	Na[a] (mmolal)	K (mmolal)	$pH_{(T,P)}$
Start		25	1		570	320	250	3.5
1	144	365	220	14.5	555	360	195	5.1
2	165	365	219	14.5	568	376	192	5.1
3	169	365	261	15.5	577	376	201	5.0
4	331	365	258	15.7	565	360	205	5.0
5	176	365	221	14.2	572	371	201	5.1
6	163	365	238	15.5	566	364	202	5.0
7	173	375	240	15.0	562	367	195	5.2
8	165	375	262	15.2	562	364	198	5.1
9	170	375	280	16.5	563	361	202	5.0
10	162	365	259	15.9	565	365	200	5.0
11	168	365	245	15.4	575	368	207	5.0
12	167	365	285	16.3	569	364	205	4.9
13	173	375	281	16.1	576	363	213	5.0
14	168	390	285	15.3	564	365	199	5.3
15	169	390	299	14.4	553	362	191	5.2
16	192	365	305	15.2	567	360	207	4.9
17	192	375	237	14.2	570	355	215	5.2
18	238	375	235	13.8	571	357	214	5.2
19	286	375	240	14.4	570	356	214	5.2
20	334	375	237	14.3	572	362	210	5.2
21	144	375	254	15.2	570	354	216	5.1
22	194	375	257	15.1	571	358	213	5.1
23	240	375	257	15.5	570	352	218	5.1
24	120	375	281	15.3	570	353	217	5.0
25	170	375	279	15.7	570	355	215	5.0
26	210	375	278	15.5	568	354	214	5.0
27	120	375	266	15.3	572	355	217	5.0
28	168	375	243	14.7	571	353	218	5.1
29	168	365	305	15.5	571	354	217	4.9
30	169	365	283	16.1	566	344	222	4.9
31	168	390	306	15.9	572	353	218	5.1
32	169	390	317	15.9	579	358	221	5.1
33	168	390	342	16.2	570	355	215	5.0
34	169	390	326	16.6	570	348	222	5.1
35	167	390	304	15.7	568	349	219	5.1
36	169	390	286	14.5	569	351	218	5.2
37	164	390	307	15.5	570	351	219	5.1
38	160	390	319	16.3	575	354	220	5.1
39	323	390	342	16.3	577	360	217	5.0
40	171	390	319	15.3	569	352	217	5.1
41	163	390	274	14.8	568	333	235	5.4
42	1032	390	345	18.0	573	396	177	5.1
43	725	390	303	14.6	578	410	168	5.3
44	168	390	305	15.7	625	406	219	5.2
45	27	390	284	15.4	577	382	195	5.3
46	54	390	285	14.8	583	382	201	5.3
47	544	390	287	14.8	578	372	206	5.3
48	792	390	284	15.2	588	385	203	5.3
49	192	390	270	13.7	716	451	265	5.4
50	123	390	267	14.3	795	535	260	5.6
51	20	390	285	14.9	633	401	232	5.3
52	144	390	285	14.7	632	411	221	5.3
53	168	390	283	14.9	629	406	223	5.3
54	192	390	283	14.9	641	420	221	5.3
55	120	390	290	15.1	658	403	255	5.2
56	144	390	287	15.0	652	393	259	5.2
57	264	390	297	15.2	658	397	261	5.1
58	384	390	281	14.6	652	392	260	5.2
59	528	390	280	14.4	633	369	264	5.2
60	552	390	279	14.7	656	402	254	5.3
61	1056	390	286	15.5	704	443	261	5.2
62	1200	390	281	15.4	696	436	260	5.3
63	144	390	286	13.7	644	421	223	5.3

(*continued on next page*)

Table 2 (*continued*)

Sample No.	Reaction time (h)	T (°C)	P (bars)	$SiO_{2(aq)}$ (mmolal)	Cl (mmolal)	Na[a] (mmolal)	K (mmolal)	$pH_{(T,P)}$
64	168	390	286	13.9	659	431	228	5.3
65	408	390	282	15.1	1135	766	369	5.2
66	192	390	293	14.4	611	447	164	5.3
67	384	390	288	14.8	613	455	158	5.4
68	312	390	282	15.4	621	415	206	5.3
69	1008	390	283	16.1	697	455	242	5.3
70	41	430	378	16.0	578	319	259	5.5
71	67	430	376	13.4	572	317	255	5.6
72	91	430	375	15.3	573	316	257	5.6
73	420	430	381	12.3	371	204	167	5.6
74	192	420	352	14.2	634	540	94	6.0
75	96	420	363	13.5	540	375	165	5.6

Data reported in sequence of sampling.
[a] Concentrations of Na were corrected based on charge balance.

Table 3
Chemical composition of fluid samples from quartz solubility experiments in the NaCl–H_2O system and in the absence of potassium bearing minerals (K–feldspar, muscovite)

Sample No.	Reaction time (h)	T (°C)	P (bars)	$SiO_{2(aq)}$ (mmolal)	Cl (mmolal)	Na[a] (mmolal)	$pH_{(25\ °C)}$
1	184	375	261	15.7	577	577	5.5
2	135	365	254	15.7	572	572	5.3
3	111	375	258	15.4	573	573	5.8
4	160	365	256	15.5	559	559	

Data reported in sequence of sampling.
[a] Concentrations of Na were corrected based on charge balance.

Table 4
Chemical composition of vapor fluids sampled from quartz solubility experiments at subcritical and supercritical conditions in the NaCl–KCl–H_2O system

Sample No.	Reaction time (h)	T (°C)	P (bars)	ΔT[a] (°C)	$SiO_{2(aq)}$ (mmolal)	Cl (mmolal)	Na[b] (mmolal)	K (mmolal)
1	72	389	251	1	3.8	69	40	29
2	72	392	241	1	2.8	18	12	6
3	120	389	250	1	3.4	71	46	25
4	720	391	254	0	3.7	43	28	15
5	288	396	241	1	2.2	15	11	4
6	216	393	251	2	2.8	30	22	8
7	156	428	350	0	14.6	437	235	202
8	180	430	352	0	12.1	289	159	130
9	276	429	350	1	10.8	335	180	155
10	240	417	322	−1	8.8	418	361	57
11	340	419	321	0	8.4	209	130	79
12	264	419	321	0	7.4	193	134	59
13	432	417	316	1	6.0	193	134	59

Data reported in sequence of sampling.
[a] Difference between measured and estimated temperatures (ΔT) at given pressure based on NaCl–H_2O phase relationships (Bischoff, 1991; Berndt et al., 2001).
[b] Concentrations of Na were corrected based on charge balance.

vapor relationships were described by the one-dimensional mathematical model *Salt-Therm 1.0* (Berndt et al., 2001).

When expressing quartz solubility using the Von Damm et al. (1991) and Fournier (1983) algorithms, density (g/cm^3) for 3.2 wt% NaCl aqueous solution were estimated from Bischoff and Rosenbauer (1985).

Statistical analysis of the experimental data and regression equations were derived through the software package *Arc 1.06* (http://www.stat.umn.edu/arc) (Cook and Weisberg, 1999). The software is functioning under Lisp-Stat (Tierney, 1989), a statistical computing environment for data analysis by making use of dynamic graphical methods.

2.3. Vent fluid samples

Vent fluid samples collected in February 2004 as part of an RV *Atlantis*/DSV *Alvin* expedition on the East Pacific Rise (EPR) between 9°50′N and 9°51′N (Fig. 2), provide

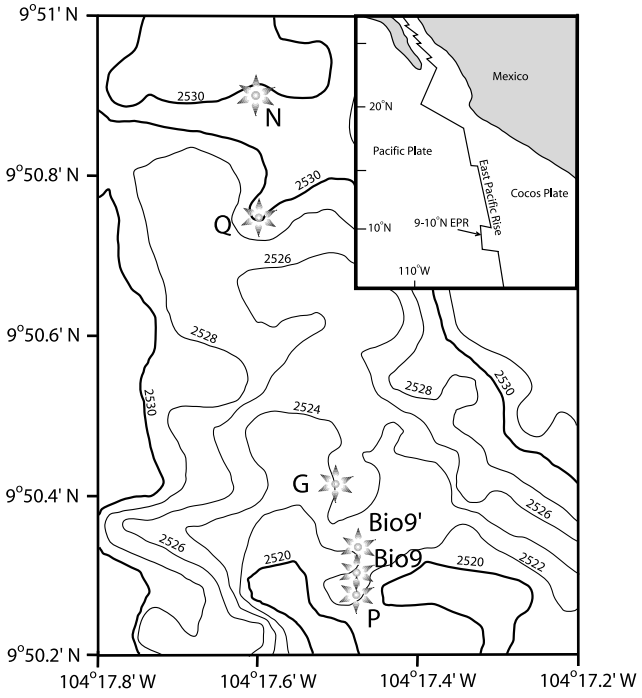

Fig. 2. Geologic map of vent sites located at 9°50′N East Pacific Rise. On February 2004, fluids were collected from P, Bio9, Bio9′, and Q vents. The map was modified after Sohn et al. (1998) and Fornari et al. (2004).

a means to test predictions based on the newly obtained quartz solubility data, while extending time series observations initiated more than a decade ago (Von Damm, 2000). This rapidly spreading section of the EPR (11 cm/yr full rate) (Carbotte and McDonald, 1992) is characterized by abundant seafloor vent sites, most at a depth of approximately 2500 m. High temperature hydrothermal activity is fuelled by a shallow magma chamber, likely located 1.2–2.4 km below the seafloor (Detrick et al., 1987; Kent et al., 1993). Seismic activity, occurring just above the melt lens and very close to the seafloor (~1 km), has also affected the temporal variability of dissolved species in vent fluids (Sohn et al., 1998).

Most hydrothermal vents are located within the axial summit collapse trough (Von Damm, 2000). Although samples were collected from Q vent, at the northern end of the segment, our efforts were largely focused at vent sites associated with the most hydrothermally active part of the 9°50′N segment, known as the "Hole-to-Hell" (Von Damm, 2004). Thus, fluid samples were obtained from vent structures at Bio9, Bio9 prime (Bio9′) and P vent (Fig. 2). Since the 1991–1992 volcanic eruptions, vent fluids from the "Hole-to-Hell' region have experienced elevated temperatures and extensive chemical variability in time and space (Von Damm, 2000; Von Damm, 2004), underscoring the impact of magmatic and tectonic events on overall heat and mass transport processes. Accordingly, monitoring the chemical evolution of these vents is essential to understand the physical and chemical evolution of submarine hydrothermal systems subsequent to a major volcanic/seismic event.

Fluid samples were collected in titanium majors bottles (Von Damm et al., 1985) and in titanium gas-tight isobaric fluid samplers (Seewald et al., 2002). Fluids were processed on board *R/V Atlantis*, and sub-samples were taken from each bottle for determination of major dissolved anions and cations, including Cl, Mg, and $SiO_{2(aq)}$ (Table 5). The aliquot used for $SiO_{2(aq)}$was immediately acidified with analytical grade HCl (Optima[7]) and diluted 100-fold to prevent mineral precipitation prior to analysis. Shore-based lab analyses were conducted by ICP-MS and ion chromatography with uncertainties similar to those reported for the experimental data.

Seawater filling dead space in fluid samplers and entrained during sampling can introduce compositional variability in the sampled fluids. Thus, composition of hydrothermal endmembers (Table 6) was calculated using a least squares regression of an individual chemical species (e.g., dissolved SiO_2) and Mg by assuming passage through the seawater composition and then extrapolating measured

Table 5
Selected element concentrations in vent fluids at 9°50′N EPR collected in February 2004

Sample[a]	Vent	Depth	T (°C)	Mg (mM[b])	Cl (mM)	$SiO_{2(aq)}$ (mM)
M3969-11	Q-vent	2503	343	50.9	562	1.7
M3969-15	Q-vent	2503		52.2	565	1.3
IGT3972-1	Q-vent	2503		4.2	581	16.9
IGT3972-4	Q-vent	2503		2.0	581	17.1
M3972-11	Q-vent	2503		29.6	571	8.7
M3972-15	Q-vent	2503		15.4	577	13.3
IGT3961-4	P-vent	2511	359	1.5	546	14.1
M3961-11	P-vent	2511		50.7	555	1.1
M3961-15	P-vent	2511		52.3	559	0.9
IGT3964-4	P-vent	2511	364	1.4	550	14.1
M3964-11	P-vent	2511		3.2	558	13.9
M3964-15	P-vent	2511		3.1	559	14.1
IGT3961-1	Bio9	2513	366	1.5	328	9.5
M3961-16	Bio9	2513		30.6	454	4.8
M3961-21	Bio9	2513		40.8	500	2.9
M3969-16	Bio9′	2513	383	3.5	292	9.1
M3969-21	Bio9′	2513		26.2	410	5.3
Dive 3970	Seawater		2	52.5	540[c]	0.2

[a] *M* and *IGT* notation refers to major and isobaric gas-tight samplers, respectively.
[b] mM = $mmol/kg_{solution}$.
[c] Data from GERM database (http://earthref.org/GERM).

Table 6
Endmember concentrations of dissolved Cl and SiO_2 in 9°50′N EPR vent fluids

Vent	T (°C)	Cl (mM[a])	$SiO_{2(aq)}$ (mM)
Q-vent	343	587	18.3
P-vent	364	554	14.7
Bio9	366	325	10.1
Bio9′	383	276	9.9

[a] mM = $mmol/kg_{solution}$.

values to zero Mg (Edmond et al., 1979). Fluids collected from the same vent orifice, when repeatedly sampled throughout the cruise, were regressed together to yield a single endmember composition.

Vent fluid temperatures were measured with the DSV *Alvin* high temperature probe and with thermocouples mounted directly on bottle snorkels. There was good correspondence between temperatures obtained using both approaches.

3. Results

3.1. Hydrothermal experiments

A total of 92 quartz solubility measurements were obtained during the experimental study (Fig. 1). As anticipated, dissolved SiO_2 concentrations increased with pressure along a given isotherm (Table 2). Moreover, dissolved SiO_2 in the Na and Na–K bearing systems (Tables 2, 3) attained nearly identical values (within analytical uncertainties), confirming that for the range of chemical and physical conditions investigated, Na and K affect similarly quartz solubility patterns. Thus, that fluids from the experiments contained dissolved Na/K ratios often different from hydrothermal vent fluids at mid-ocean ridges is unlikely to affect dissolved SiO_2 concentrations in fluids coexisting with quartz, provided ionic strength effects are explicitly taken into account. Increasing proximity to the two-phase boundary, however, caused a noticeable decrease in dissolved SiO_2, although even upon intersection with this boundary, significant dissolved SiO_2 concentrations were still observed for both subcritical and supercritical vapor-rich fluids (Table 4).

3.2. Vent fluids from 9°50′N EPR

A total of 15 vent fluid samples were collected in February 2004, at P, Bio9, and Bio9′ vent structures at 9°50′N EPR (Fig. 2). These vent sites have been visited frequently over the years (Von Damm, 2000; Von Damm, 2004), ever since a magmatic eruption affected the hydrothermal system (Haymon et al., 1993). Vent fluids were also sampled at the Q site, in the northern region of the study area, the chemical composition of which has not been reported since 1994 (Oosting and Von Damm, 1996). In general, chemical and temperature data collected in the 9°50′N EPR region (Tables 5–7) demonstrate the dynamic nature of subseafloor hydrothermal systems, where abrupt magmatic/tectonic events can trigger corresponding changes in overlying hydrothermal systems (Sohn et al., 1998; Von Damm, 2000).

These and other data indicate that vent fluid systems located at the "Hole-to-Hell" area have higher temperatures than in the northern part of the 9°50′N EPR region, such as at the Q-vent. Indeed, that was the case in 2004, where fluids issuing from P, Bio9, and Bio9′ vent structures were approximately 30–40 °C higher than at the Q-site (Table 5). Temperatures measured at Q-vent site contrast with the maximum temperature of 371 °C recorded just after the 1991–1992 volcanic eruptions (Table 7).

Table 7
Time series data for selected aqueous species in 9°50′N EPR vent fluids collected in the aftermath of the 1991 volcanic eruption

Vent	Date	T (°C)	Cl (M[a])	$SiO_{2(aq)}$ (mM)	Ref.
N.1	April 1991	325	0.036	3.3	[b]
Q.1	April 1991	371	0.071	7.5	[b]
G.1	April 1991	326	0.150	8.5	[b]
G.2	April 1991	355	0.154	6.5	[b]
B9.1	April 1991	368	0.154	9.9	[b,c]
B9.2	March 1992	>388	0.076	7.0	[c]
B9.3	December 1993	365	0.212	11.3	[c]
B9.4	March 1994	359	0.263	12.1	[c]
B9.5	March 1994	363	0.267	12.6	[c]
B9.6	October 1994	363	0.325	13.9	[c]
B9.7	October 1994	359	0.330	14.1	[c]
B9.8	November 1995	364	0.498	14.8	[c]
B9.9	November 1997	373	0.400	13.2	[c]
B9.10	November 1997	371	0.401	12.8	[c]
B9.11	May 1999	365	0.348	11.7	[c]
B9.12	April 2000	379?	0.306	11.0	[c]
B9.13	February 2002	386	0.226	8.2	[c]
B9′.1	March 1994	361	0.249	12.4	[c]
B9′.2	October 1994	361	0.330	14.0	[c]
B9′.3	October 1994	364	0.332	13.3	[c]
B9′.4	November 1995	366	0.466	14.5	[c]
B9′.5	April 1996	367	0.501	15.1	[c]
B9′.6	November 1997	358	0.473	13.4	[c]
B9′.7	November 1997	364	0.473	14.9	[c]
B9′.8	May 1999	376	0.349	11.7	[c]
B9′.9	April 2000	330	0.257	11.8	[c]
B9′.10	January 2002	386	0.217	8.0	[c]
B9″.1	January 2002	377	0.243	8.6	[c]
B9complex	December 1999	378	0.390	12.5	[c]
P.1	April 1991	369	0.135	8.7	[b,c]
P.3[d]	March 1992	392	0.043	3.7	[b,c]
P.4	March 1992	392	0.042	3.9	[c]
P.5	December 1993	364	0.262	12.3	[c]
P.6	March 1994	350	0.347	14.2	[c]
P.7	March 1994	377	0.352	14.3	[c]
P.8	October 1994	359	0.530	16.2	[c]
P.9	November 1995	360	0.622	15.8	[c]
P.10	November 1995	357	0.566	16.2	[c]
P.11	November 1995	367	0.620	16.4	[c]
P.12	April 1996	367	0.587	16.6	[c]
P.13	April 1996	368	0.584	16.0	[c]
P.14	November 1997	372	0.529	15.3	[c]
P.15	November 1997	379	0.512	15.6	[c]
P.16[d]	December 1997	378	0.519	15.1	[c]
P.17[d]	December 1997	378	0.528	15.4	[c]
P.18	May 1999	374	0.500	14.2	[c]
P.19	May 1999	377	0.517	15.7	[c]
P.20	May 1999	375	0.512	14.9	[c]
P.21	December 1999	382	0.505	14.7	[c]
P.22	April 2000	383	0.517	14.4	[c]
P.23	January 2002	386	0.530	13.0	[c]
P.24	January 2002	385	0.531	12.8	[c]
P.middle	January 2002	383	0.518	12.8	[c]
P.middle	January 2002	385	0.519	12.6	[c]

The B9.x notation refers to the Bio9 vent area.
[a] $M = mol/kg_{solution}$.
[b] Von Damm (2000).
[c] Von Damm (2004).
[d] Dissolved Cl concentrations estimated by charge balance.

Elevated fluid temperatures and spatial variability of dissolved Cl suggest that phase separation effects play a key role in heat and mass transport in the 9°50′N EPR hydrothermal system. Vent fluids from structures at Q and P have endmember chloride concentrations of 587 and 554 mmol/kg_{sol}, respectively (Table 6). On the other hand, Bio9 and Bio9′ vent fluids are vapor-rich with Cl concentrations of 325 and 274 mmol/kg_{sol}. Despite being in close proximity, the Bio9 complex reveals vent fluids with dissolved chloride concentrations lower than at the P site, suggesting a different set of P–T conditions in their respective subseafloor reaction zones (Von Damm, 2004).

Assuming equilibrium with quartz, it is possible to constrain temperatures and pressures from dissolved chloride and silica concentrations in the coexisting aqueous fluid (Fournier, 1983; Von Damm et al., 1991). In the case of the Cl-depleted Bio9 and Bio9′ vent fluids, $SiO_{2(aq)}$ concentrations are 10.1 and 9.9 mmol/kg_{sol}, respectively. The Cl-enriched fluids from P and Q vents, however, are characterized by higher dissolved silica concentrations of 14.7 and 18.3 mmol/kg_{sol}. The relatively elevated $SiO_{2(aq)}$ concentrations in these vent fluids are mostly the result of *salting-in* effects in NaCl-bearing fluids at high temperature and low pressure conditions (Fournier, 1983; Von Damm et al., 1991; Xie and Walther, 1993). As noted previously, however, the dearth of experimental quartz solubility data at temperature, pressure and compositional conditions most relevant to the 9°50′N EPR region render uncertain estimates of temperature and pressure using available quartz solubility algorithms.

4. Discussion

4.1. Modeling quartz solubility at near critical conditions

It is well known that quartz solubility depends on pressure, temperature and dissolved chloride of the aqueous fluid, manifest by changes in thermodynamic properties and in the activity coefficient of dissolved SiO_2 (Khitarov, 1956; Kitahara, 1960; Anderson and Burnham, 1967; Ganeyev, 1975; Hemley et al., 1980; Chen and Marshall, 1982; Fournier et al., 1982; Fournier, 1983; Saccocia and Seyfried, 1990; Von Damm et al., 1991; Xie and Walther, 1993; Newton and Manning, 2000; Shmulovich et al., 2001). In general, when the activity coefficient of dissolved SiO_2 is less that unity, quartz solubility increases (*salting-in*), while the opposite is true for activity coefficients greater than unity (*salting-out*).

Several mechanisms have been proposed to account for the effect of dissolved chloride concentrations on quartz solubility in moderately acidic fluids. In all the cases, silicic acid (H_4SiO_4) is considered to be the dominant dissolved silica species (Walther and Helgeson, 1977). Thus, Anderson and Burnham (1967, 1983) and Seward (1974) proposed that ionization of the silicic acid and successive association with alkalies (e.g., Na^+), would form aqueous alkali silica hydrous complexes as follows:

$$\text{Quartz} + H_2O = H_4SiO_{4(aq)} \quad (5)$$

$$H_4SiO_{4(aq)} + NaCl = H_3NaSiO_4 + HCl \quad (6)$$

Recent mineral solubility studies (Newton and Manning, 2000) and *in-situ* Raman spectroscopy analysis of $SiO_{2(aq)}$ species (Zotov and Keppler, 2000), however, strongly suggest that de-protonation of H_4SiO_4 is limited, weakening the theory of alkali silica hydrous complexes formation during quartz dissolution in Cl-bearing fluids.

Accordingly, the presence of abundant H_4SiO_4 (i.e., $SiO_{2(aq)}$) in chloride enriched brines, as compared to pure H_2O, indicate that *salting-in* effects result mainly from short-range electrostatic interactions between neutral $SiO_{2(aq)}$ and coexisting charged species (Xie and Walther, 1993). Thus, in order to describe quartz solubility unambiguously, the collective effects of solvation and short-range electrostatic interactions need to be considered. This is typically accomplished by use of the Setchenow equation (Eq. (4)). Experimentally reported Setchenow coefficients for $SiO_{2(aq)}$ range from 0.028 kg/mol (*salting-out*) to −56.7 kg/mol (*salting-in*) (Xie and Walther, 1993), with the highest negative values for low density fluids, underlining the dominant effect of short-range electrostatic interactions on quartz solubility at P–T conditions near and beyond the critical point for NaCl-fluids, such as seawater (Newton and Manning, 2000).

Salting-in effects anticipated for quartz solubility in high temperature and low to moderate pressure submarine hydrothermal fluids can be expressed in forms analogous to that presented earlier in Von Damm et al. (1991), which covers a relatively broad range of pressure and temperature space, but is largely limited in composition space to 3.2 wt% NaCl and pure water systems. These investigations proposed an equation having the following form:

$$\ln m_{SiO_{2(aq)}} = a + b\ln\rho + (c + dT^2)T^{-1} + ePT^{-1} \quad (7)$$

where a, b, c, d, and e[3] are fitting coefficients, T is temperature in °K, P is pressure in bars, while ρ is the density of the fluid. The algorithm incorporates the weight fraction of free water and the activity coefficient of $SiO_{2(aq)}$ in the "a" term. In its original form (Von Damm et al., 1991), the activity coefficient of $SiO_{2(aq)}$ was considered similar for seawater (3.2 wt% NaCl) and pure water, likely limiting more general applications. The algorithm (7), however, has been shown to accurately predict dissolved SiO_2 in pure H_2O at elevated pressures and temperatures (Gunnarsson and Arnorsson, 2000)—a result that relates in part to the greater availability of quartz solubility data for pure water systems, from which fitting coefficients for expression (7) were derived. Thus, we have elected to use this algorithm to calculate dissolved silica concentrations in H_2O

[3] a = −2.32888, b = 1.79547, c = −2263.62, d = 0.00407350, e = 0.0398808.

($m_{SiO_{2(aq)},o}$), when the activity coefficient of $SiO_{2(aq)}$ is likely unity, but for Cl-bearing solutions, the Setchenow equation is used as well to better constrain departures from ideality, as follows:

$$\log m_{SiO_{2(aq)}} = \log m_{SiO_{2(aq)},o} - b_{SiO_{2(aq)}} I \quad (8)$$

where $b_{SiO2(aq)}$ is the Setchenow coefficient for $SiO_{2(aq)}$ dissolved in a NaCl-bearing aqueous fluid, which, as noted earlier, accounts mainly for ion-solvent interaction effects (Walther, 1997). As with Eq. (4), I refers to the true ionic strength.

Table 8
Data collected during quartz solubility experiments in the NaCl–H_2O system and at P–T conditions closely related to those of the present experimental study

T (°C)	P (bars)	$SiO_{2(aq)}$ (mmolal)	Cl (molal)
Fournier et al. (1982)			
350	200	17.7	2
350	238	18.4	2
350	300	18.6	2
350	340	19.0	2
350	400	18.8	2
350	180	18.2	3
350	200	17.8	3
350	220	18.4	3
350	260	19.2	3
350	300	18.9	3
350	300	19.4	3
350	380	19.6	3
350	400	20.0	3
350	400	20.4	3
350	180	18.4	4
350	200	19.0	4
350	215	18.9	4
350	220	18.4	4
350	245	18.8	4
350	260	18.7	4
350	300	19.0	4
350	300	19.3	4
350	320	19.6	4
350	320	19.1	4
350	400	19.9	4
350	400	19.7	4
Von Damm et al. (1991)			
363	280.1	16.52	0.566
363	260.9	16.29	0.566
363.5	260.8	16.33	0.566
364.6	263.9	16.33	0.566
366.4	297.6	16.56	0.566
363.3	301.6	16.87	0.566
363.6	304	16.98	0.566
364	298	17.95	0.566
362	252	17.42	0.566
363	249	17.14	0.566
363	219	16.79	0.566
361	200	16.37	0.566
362	301	16.67	0.566
361	289	16.44	0.566
362	303	16.71	0.566
362	301	16.63	0.566
361	348	17.3	0.566
398.6	317.2	14.29	0.566
403.4	315.8	14.35	0.566
397.7	344.6	16.9	0.566
396	391.2	18.37	0.566

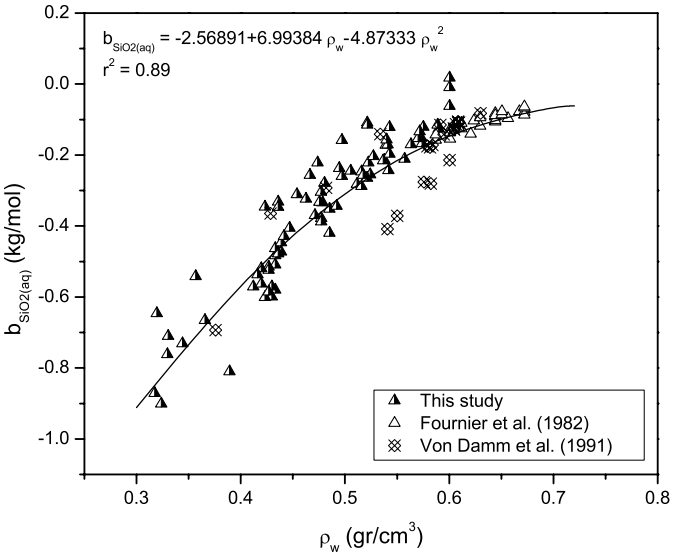

Fig. 3. Setchenow coefficients determined from quartz solubility experiments in NaCl–KCl bearing fluids at conditions that correspond to water density between 0.3 and 0.7 g/cm^3. The lack of experimental data in the near-critical region prior to current study is clearly illustrated. The quadratic linear relationship between $b_{SiO2(aq)}$ and density of pure H_2O (ρ_w) is expressed with a regression correlation coefficient (r^2) of 0.89. The decrease in $b_{SiO2(aq)}$with decreasing density, indicates enhancement of *salting-in* effects near the critical region, consistent with previous experimental observations (Xie and Walther (1993)).

Although our experiments were conducted in NaCl–KCl-bearing solutions, ion-solvent effects for Na^+ and K^+ were considered to be equal, because of their similar electrostatic (Helgeson et al., 1981) and dielectric properties (Chandra, 2000). Moreover, that we observed similar quartz solubility in NaCl and NaCl–KCl fluids of the same ionic strength provides further evidence that Na and K interact similarly with the solvent (H_2O) for the range of conditions studied (Tables 2 and 3). In general, this finding is consistent with previous experimental mineral solubility studies (Hemley et al., 1980; Marshall and Warakomski, 1980; Anderson and Burnham, 1983) and the resemblant effects of Na and K on quartz dissolution kinetics (Dove and Crerar, 1990; Dove and Nix, 1997).

Dissolved SiO_2 concentrations measured in the NaCl–KCl–SiO_2–H_2O system (Tables 2, 3, and 8) constrain $b_{SiO2(aq)}$ at near critical conditions. These data, together with the true ionic strength (I) and $m_{SiO_{2(aq)},o}$ (Von Damm et al., 1991) can be used to retrieve Setchenow coefficients for $SiO_{2(aq)}$ as a function of the density of water (ρ_w) (Fig. 3):

$$b_{SiO_{2(aq)}} = -2.56891 + 6.99384\rho_w - 4.87333\rho_w^2 \quad (9)$$

In general, this relationship[4] is valid for fluid (H_2O) density between 0.3 and 0.7 g/cm^3, corresponding to ranges in tem-

[4] Correlation coefficient $r^2 = 0.89$. Estimated standard deviation of the fitting curve (Root-MSE) = 0.0685.

perature and pressure of 350–430 °C and 200–400 bars, respectively. The decrease of $b_{SiO2(aq)}$ at low density conditions (Fig. 3), however, indicates that *salting-in* effects increase as critical conditions are approached. Overall, Setchenow coefficients determined from Eq. (9) are in good agreement with values reported by Xie and Walther (1993), where significantly negative $b_{SiO2(aq)}$ values are indicated for water density below 0.3 g/cm^3, suggesting even greater *salting-in* effects under these conditions.

Taking account of $b_{SiO2(aq)}$, quartz solubility data can be predicted. These data, however, contrast with comparable data derived from available empirical equations for quartz solubility (Fournier, 1983; Von Damm et al., 1991), owing to differences in the treatment of activity–concentration relations for dissolved $SiO_{2(aq)}$ and the range of chemical and physical conditions for which the regressions apply. For example, assuming a 3.2 wt% NaCl fluid (seawater) at temperatures less than 400 °C, the empirically based algorithms predict pressures that are 10 to 50 bars lower than indicated from results of the present study (Fig. 4). Alternatively, if pressure is fixed, lower temperatures are needed to generate dissolved silica concentrations consistent with present experimental results. At temperatures greater than 400 °C, however, the quartz solubility model developed here shows a reverse trend, indicating temperatures approximately 10 °C higher than suggested from the algorithms. These slight but significant differences have important implications for understanding the chemical evolution of the well-studied vent fluids at 9°50′N EPR.

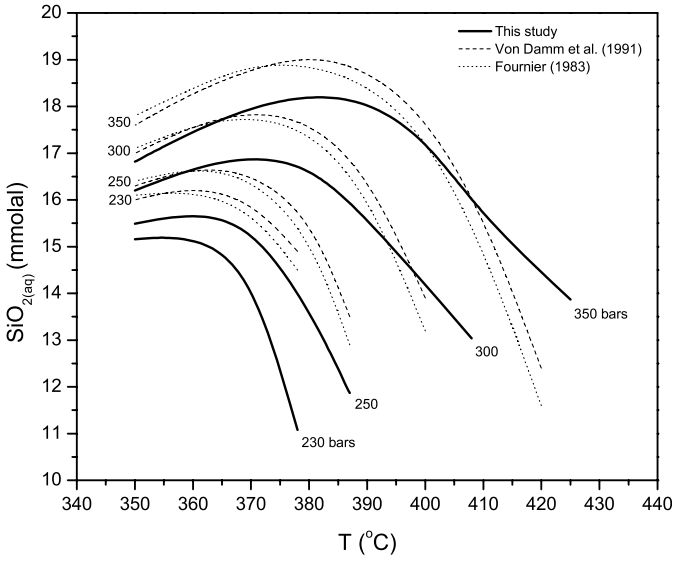

Fig. 4. The effect of temperature and pressure on dissolved silica concentrations in 3.2 wt% NaCl aqueous solutions predicted from quartz solubility algorithms derived by Fournier (1983); Von Damm et al. (1991) and from this study. The present model, which is based on new data for the activity coefficients of $SiO_{2(aq)}$ departs significantly from previous models, especially at relatively low pressures and temperatures in excess of 400 °C.

4.2. The 9°50′N EPR vent fluids in the aftermath of the 1991–1992 eruption events

As mentioned earlier, the lack of quartz solubility data at conditions beyond the two-phase boundary of seawater has been a key limitation in constraining temperature or pressure from dissolved SiO_2 concentrations in Cl-bearing vapor-rich vent fluids. It is well known that during seawater circulation near magmatic heat sources within the oceanic crust, phase separation occurs, resulting in formation of vapor and brines. Due to their relatively low density, vapors would ascend, while brines would be expected to accumulate, forming a brine layer located in a region of hot rock adjacent to the magmatic body (McNabb and Fenner, 1985; Bischoff and Rosenbauer, 1989). Moreover, recent hydrologic models suggest further that elevated pressure gradients within the upflow zone may allow brines to ascend as well, but at significantly lower flow rates than the vapors, permitting phase segregation to occur (Fontaine and Wilcock, 2006). The distribution and abundance of vents at 9°50′N EPR, which are issuing fluids with relatively low chloride concentrations (Von Damm et al., 1995; Oosting and Von Damm, 1996; Von Damm, 2000; Von Damm, 2004), confirm the role of phase separation and vapor rise on hydrothermal alteration processes for this region of the oceanic crust (Berndt and Seyfried, 1997). Thus, vent fluids at 9°50′N EPR are particularly well suited for application of the new quartz solubility data. This takes on added significance in light of the unusually complete time series data for vent fluid chemistry at 9°50′N subsequent to the seafloor volcanic eruptions that affected the area in 1991–1992 (Haymon et al., 1993; Rubin et al., 1994; Von Damm, 2000; Von Damm, 2004).

In contrast with the thermodynamically based approach used to interpret quartz solubility in 3.2 wt% NaCl fluid (see above), unusually low fluid density associated with two-phase phenomena at subcritical and supercritical conditions in the NaCl–H_2O system preclude a similar approach without introduction of unacceptably large uncertainties. Indeed, limitations in knowledge of chemical and physical properties of Na and K-bearing aqueous species at relatively low and high pressure and temperature conditions, respectively (Ho et al., 1994, 2000a,b, 2001), make calculation of true ionic strength and derivative properties highly uncertain. The abundance of quartz solubility data for vapor-rich fluids derived from subcritical and supercritical phase separation experiments (Table 4), however, allows an alternative empirical approach involving derivation of an algorithm that expresses quartz solubility in terms of temperature (T_c) (°C), molality of dissolved chloride (m_{Cl}) and density of pure H_2O (ρ_w) (g/cm^3), as follows:

$$\log m_{SiO_{2,(aq)}} = -5.10347 + 0.00883565T_c + 0.105367 \times \log m_{Cl} + 1.03419 \log \rho_w \quad (10)$$

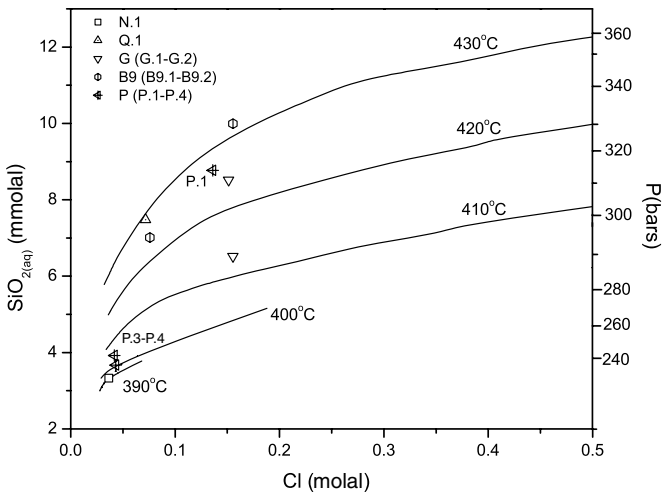

Fig. 5. Dissolved silica concentrations in vapor-rich vent fluids at 9–10°N EPR in comparison with quartz solubility data predicted based on models (Eq. (10)) described in this study. Significant *salting-in* effects are indicated for Cl-bearing supercritical vapors. Thus, fluids issuing from Q, G, P, and Bio9 vents in the aftermath of the 1991–1992 volcanic event (Table 7), suggest temperatures of 420-430 °C and pressures between 310 and 340 bars. Unusually Cl-depleted vent fluids (P.3, P.4, and N.1), however, do not permit unambiguous determination of *P–T* conditions, allowing the possibility of higher temperatures. Vent fluid compositions have been converted to molal units to conform better to experimental data. Pressure (second *y*-axis) corresponds to conditions imposed by the composition of the vapor phases (*x*-axis) depicted by the solid lines, assuming equilibrium in the NaCl–H_2O system (Berndt et al., 2001).

The empirical Eq. (10)[5] describing quartz solubility in vapor-rich fluids is valid for water density ranging from 0.16 to 0.28 g/cm^3, which corresponds to pressures from 235 to 360 bars and temperatures between 390 and 430 °C. As expected, supercritical conditions significantly enhance quartz solubility relative to the subcritical conditions (Fig. 5). During subcritical phase separation, vapors with dissolved Cl concentrations less than 50 mmolal contain $SiO_{2(aq)}$ concentrations virtually identical to the concentrations predicted for the pure H_2O system. With increase in chlorinity and temperature (formation of supercritical vapors), however, dissolved silica concentrations begin to deviate substantially from the chloride-free fluids.

The extraordinary depletion in dissolved Cl in hydrothermal fluids issuing from vents at 9°50′N EPR in the immediate aftermath of seafloor volcanic eruptions in 1991 and 1992 has been interpreted as a result of phase separation, likely occurring very near the seafloor (Von Damm, 2000; Von Damm, 2004). Indeed, dissolved chloride concentrations and temperature reported for these fluids range from approximately 36 to 154 mmol/kg$_{sol}$ and 325 to 392 °C, respectively, where higher temperatures are associated with lower dissolved chloride (Table 7). Dissolved silica concentrations, however, were not primarily used to constrain subseafloor pressure/temperature conditions owing to the likelihood that these conditions would fall outside the confidence interval of quartz solubility data available at the time. Thus, pressure and temperature conditions for phase separation were mainly inferred from phase relations in the NaCl–H_2O system (Von Damm, 2004). For example, assuming vent fluids temperatures (adjusted for likely adiabatic and conductive cooling effects), Von Damm (2004) inferred subcritical conditions of phase separation, with a location situated less than 200 m below seafloor (255–270 bars). Owing to uncertainties related to the extent of subseafloor cooling, however, a wide range of *P–T* conditions can be described for the cause of chloride variations in the vapor-rich vent fluids (Bischoff, 1991; Berndt et al., 2001).

Using data and equations from the present study, dissolved SiO_2 concentrations in the vent fluids can now be used to constrain the depth (pressure) and temperature of fluid circulation, as expressed by Eq. (10). Accordingly, the Cl-depleted and $SiO_{2(aq)}$-enriched vapors reported for Bio9, G, and Q vents at 9°50′N EPR following the 1991–1992 volcanic eruptions, suggest supercritical phase separation processes (Fig. 5). Specifically, fluid samples B9.1 and B9.2, having dissolved SiO_2 of 10 and 7 mmol/kg$_{sol}$, respectively (Table 7), indicate temperatures of between 420 and 430 °C at a depth of 600–900 m (310–340 bars) within the oceanic crust. Moreover, the elevated $SiO_{2(aq)}$ concentrations of Q vent fluid (Q.1) indicate temperatures close to 430 °C and pressure of nearly 315 bars, while dissolved SiO_2 and chloride of hydrothermal fluid issuing from G vent suggest lower temperatures, yet similar pressures, but in all cases still within the supercritical region (Fig. 5). P vent fluid, however, reveals a more complex pattern, with the first sample (P.1) indicating supercritical *T–P* conditions (~430 °C, 330 bar), while subcritical conditions are suggested by subsequent vent fluid samples (P.3–P.4), with temperatures close to 400 °C and pressures in keeping with previous estimates (Von Damm, 2004). The unusually low dissolved chloride concentrations characterizing P (P.3–P.4) and N (N.1) vent fluids, however, inhibit quartz solubility owing to limited *salting-in* effects. Thus, under these conditions, it is difficult to resolve unambiguously *P–T* conditions allowing the possibility of higher temperatures (similar to P.1 sample), although low pressure conditions can not be avoided (Fig. 5). In general, the 1991–1992 volcanic eruptions appear to be responsible for extensive heat transfer across the 9°50′N EPR hydrothermal system, subjecting seawater derived hydrothermal fluids to supercritical conditions for a significant portion of the monitoring interval.

4.3. Quartz solubility constraints for the evolving 9°50′N EPR system

Time series observations of vent fluid samples collected from 1993 until 2004 at 9°50′N EPR indicate a general increase in dissolved chloride and decrease in temperature

[5] Correlation coefficient $r^2 = 0.96$. The distribution of regression residuals follows the assumption of normality, without deviating from a random sample of a normal distribution in any systematic manner.

(Tables 6, 7). For example, dissolved chloride concentrations of vent fluids issuing from the Bio9 area (Bio9, Bio9′, Bio9″, and Bio9complex) reveal values less than seawater, with the highest concentrations (~0.5 mol/kg_{sol}) observed following the seismic swarm of 1995 (Sohn et al., 1998). Hydrothermal fluids issuing from P vent also indicate an abrupt increase in Cl during that time (0.622 mol/kg_{sol}), although chloride concentrations failed to depart significantly from seawater-like values subsequently, further suggesting that subseafloor reaction zones responsible for Bio9 area and P vent fluids are distinct (Sohn et al., 1998; Von Damm, 2004). Seismic data indicate that the 1995 event occurred at ~1 km below seafloor (Sohn et al., 1998), while significantly altering vent-fluid composition and temperature of the 9°50′N EPR hydrothermal system (Fornari et al., 1998; Sohn et al., 1998; Von Damm, 2004). One interpretation of this involves the seismically induced downward propagation of a network of cracks that allowed fluid to access deeper portions of the crust. Accordingly, the higher subseafloor pressure would permit higher dissolved chloride concentrations owing to the effect of temperature and pressure on phase relations in the NaCl–H_2O system. By this model, the relatively low vent fluid temperatures could be interpreted to result from cooling effects associated with the greater travel path to seafloor (Sohn et al., 1998; Von Damm, 2004). Taking account of dissolved chloride concentrations together with other imposed constraints, Von Damm (2004) estimated that the 9°50′N EPR vent fluid source-region did not experience temperatures and pressures in excess of the critical point of a 3.2 wt% NaCl fluid, with the only exemption being P vent fluids where estimated temperatures reached values of 409 °C after the seismic event of 1995.

Estimates of the conditions in subseafloor reaction zones at 9°50′N EPR based on quartz solubility data reported earlier indicate predominance of supercritical conditions at sub-crustal depths greater than 0.5 km. In order to apply quartz–fluid equilibria (Eq. (10)) to the vapor endmembers with minimum uncertainties, however, we limited our analysis to vent fluids with chloride concentrations less than 450 mmolal, reflecting the range of salinities measured in phase separation experiments (Table 4). In contrast, vent fluids with dissolved Cl greater than or equal to seawater values were treated together using the $b_{SiO2(aq)}$ approach discussed earlier (Eq. (8)). Thus, samples from Bio9 area are considered vapors; excluding fluids collected in 1994–1997 (B9.8, B9′.4–B9′.7), all of which exhibit relatively elevated Cl concentrations.

Bio9 and P hydrothermal systems appear to follow distinctly different evolutionary pathways. As previously noted, subsequent to the 1991–1992 volcanic eruption, fluids from both vent sites reflect supercritical conditions, as suggested by the coexistence of low chloride vapors and elevated $SiO_{2(aq)}$ concentrations. In subsequent years, however, hydrothermal fluids venting at the P site indicate increasing pressures without significant change in measured temperature. Indeed, from quartz solubility constraints, the relatively high Cl and $SiO_{2(aq)}$ concentrations suggest temperatures near 430 °C, and pressures in excess of 360 bars (Fig. 6a), conditions very close to the critical curve for the NaCl–H_2O system (Bischoff, 1991; Berndt et al., 2001). Thus, the 1995 seismic event must have facilitated downward penetration of fluid, likely owing to the existence of a more permeable network of cracks. The post 1995 seawater-like vent fluids issuing from P vent have relatively high dissolved silica concentrations suggesting temperatures of 400–420 °C and pressures between 350 to 400 bars (Fig. 6b). Therefore, it appears that phase separation effects result in vapor and brine compositions that depart only slightly from the dissolved chloride of seawater (Bischoff, 1991; Berndt et al., 2001), which in turn enhances dissolved SiO_2 concentrations.

In contrast with the role of pressure on phase separation and composition of the P-vent fluid, the Bio9 area vent fluids appear to be influenced more by perturbations of the heat source. Quartz–fluid equilibria data suggest that prior to the 1995 seismic event, the system experienced elevated temperatures (430 °C) and pressures progressively increasing from 310 to 360 bars, producing Cl-bearing supercritical vapors containing nearly 14 mmolal SiO_2 (Fig. 6a). Pressure estimates are consistent with the projected location of hypocenters of the microseismic event at 1–1.2 km in the oceanic crust (Sohn et al., 1998). Decreases in Cl and $SiO_{2(aq)}$ concentrations in years following the seismic event, however, have been linked to an upward migration of the heat source (Von Damm, 2004). Our data support this interpretation recognizing that measured dissolved $SiO_{2(aq)}$ and Cl indicate pressures close to 320 bars, which correspond to a 40 bars (400 m) decrease in pressure (Fig. 6a). Temperature estimates, however, remain in the vicinity of 420 °C. Thus, the evolution of the Bio9 hydrothermal system vent fluid based on constraints imposed by quartz–fluid equilibria, involves water/rock interactions at supercritical temperatures of 420–430 °C and pressures ranging from 310 bars up to 380 bars (Figs. 6a and b). These results are consistent with models based on the initial short-lived temperature increase in the Bio9 area (Wilcock, 2004). In general, this thermo modeling approach makes use of perturbations in the temperature of fluids sampled immediately after the 1995 seismic event (Fornari et al., 1998), indicating a 50 °C increase of basal temperature, placing the subseafloor reaction zone within the supercritical region and at a temperature regime in excess of 420 °C.

The proposed origin of vent fluids issuing from P and Bio-9 area involves supercritical phase separation effects at temperatures of 420–430 °C and pressures equivalent to depths between 600 and 1500 m. Accordingly, brine storage likely occurs above the interface of the hydrothermal/magmatic boundary, allowing more or less continuous venting of vapor-rich fluids. Formation of neutrally buoyant brine pools (Fontaine and Wilcock, 2006) requires indeed significant depths to accommodate storage of high salinity fluids. Nevertheless, supercritical conditions are

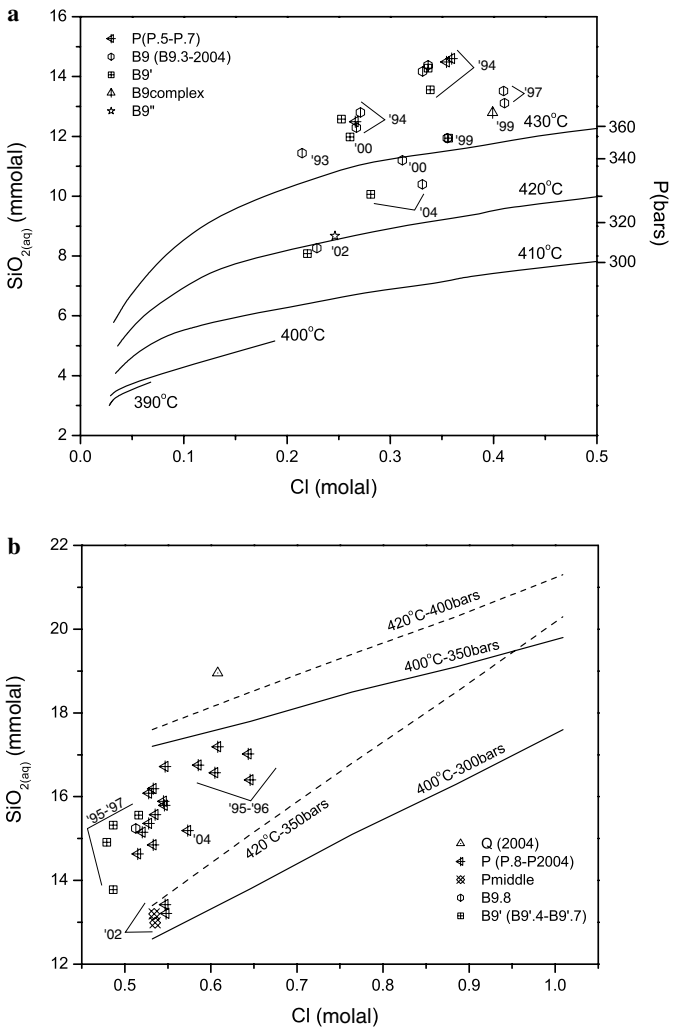

Fig. 6. Dissolved silica concentrations predicted for vapor-rich (two-phase system) (a) and homogeneous (one-phase system) Cl-bearing fluids (b), as a function of temperature and dissolved chloride in comparison with hydrothermal vent fluids at 9°50′N EPR (Tables 6 and 7). Assuming quartz–fluid equilibria, vent fluids collected in years following volcanic eruptions (1991–1992), indicate changes in temperature and pressure (as reflected by changes in dissolved silica) that can be linked to tectonic/seismic events. Vapor-rich fluids sampled prior to the 1995 seismic events (a) reveal a relatively deep hydrothermal reaction zone characterized by pressures greater than 360 bars and temperatures in excess of 430 °C (supercritical). The seismic event of 1995, however, enhanced crustal permeability, causing fluids to penetrate to even greater depths as indicated by time series observations on vent fluid changes in dissolved silica and Cl concentrations. For Bio9 vent fluids sampled subsequent to the seismic event, further deepening of the reaction zone is not indicated. Indeed, based on time series changes in chloride and $SiO_{2(aq)}$, pressures as low as 320 bars are suggested for the Bio9 vent fluids, which may actually be a response to upwards migration of melt. If this is the case, however, it had little effect on the P vent fluid system (b). Throughout the 1995–2004 interval the subseafloor pressure predicted for the P-vent fluid fluctuated between 350 bars and ~380 bars, while temperatures were sustained at values of approximately 420 °C. In contrast, hydrothermal fluids issuing at the Q-site (b) reveal cooling and deepening since 1991, with the more recent (2004) temperature–pressure conditions being approximately 400–420 °C and 400 bars.

more plausible in a long-term phase separated hydrothermal system, with an axial magma chamber located just underneath the subseafloor reaction zone (W.S. Wilcock, personal communication). Cooling of the system owing to decay of the magmatic heat source would allow penetration of evolved seawater and mixing with the brine layer, which would eventually permit venting of higher chloride fluid. Frequent magmatic intrusions, however, associated with the fast-spreading nature of the East Pacific Rise would most likely continue to maintain high rates of heat flux observed more recently (2004).

5. Conclusions

Experiments were conducted to investigate quartz solubility at conditions particularly applicable to shallow subseafloor hydrothermal systems at mid-ocean ridges, where phase separation processes are known to occur. Accordingly, the experiments were preformed in aqueous Cl-bearing fluids at temperatures ranging from 365 to 430 °C and pressures from 219 to 381 bars, which include the critical and the two-phase region of seawater-derived hydrothermal fluids. Results reveal that dissolved SiO_2 concentrations increase with pressure at constant temperature. The magnitude of this, however, decreases with increasing proximity to the two-phase boundary in the NaCl–H_2O system. Upon intersection of the two-phase boundary, though, significant dissolved SiO_2 remains in solution for vapor-phase fluids at both subcritical and supercritical conditions. Thus, for these fluids, dissolved silica concentrations ranged from 2.81 to 14.6 mmolal, increasing with dissolved chloride concentration. The effect of dissolved chloride on quartz–fluid equilibria in the low-pressure near critical region largely results from changes in non-ideal activity–concentration relations for dissolved silica, underscoring the need to explicitly account for this in algorithms developed to predict temperature and/or pressure from dissolved silica in NaCl-bearing aqueous fluids at elevated temperatures and pressures.

Experimental results together with measurements of dissolved silica in vent fluids recently sampled (2004) at 9°50′N EPR allow more rigorous interpretation of conditions controlling the temporal evolution of subseafloor reaction zones affecting this hydrothermally active region. When combined with previously reported measurements of dissolved silica, chloride and temperature, the 2004 dataset together with experimental results confirm important time series changes largely involving processes of supercritical and near-critical phase separation. Despite differences in seismic and tectonic events at 9°50′N EPR, water/rock interactions appear to occur most often at temperatures ranging from 420 to 430 °C and at depths of 600 to 1500 m below seafloor.

Supercritical conditions in the NaCl–H_2O system are also suggested for vent fluids throughout the 9–10°N EPR region, when dissolved chloride effects are accounted for. For example, vapor-rich fluids issuing from L and A vents at 9°46′N indicate dissolved chloride concentrations between 30 and 110 mmol/kg_{sol} (Von Damm et al., 1995; Von Damm, 2000). The measured dissolved SiO_2

concentrations of nearly 7 mmol/kg_{sol}, however, require temperatures and pressures of 410–420 °C and 300 bars, respectively, assuming quartz–fluid equilibria (see Fig. 5). Supercritical phase separation conditions are also suggested for F site vent fluid at 9°16′N EPR, where dissolved Cl and SiO_2 concentrations are analogous to A and L vent fluids (Von Damm, 2000).

The newly obtained quartz solubility data together with high resolution time series measurements of vent fluid chemistry provide the requisite constraints to understand better the relative roles of magmatic and tectonic processes on the temporal evolution of subseafloor hydrothermal systems at mid-ocean ridges.

Acknowledgments

We thank the ALVIN Group, the captain and the crew of the R/V Atlantis for their help and assistance while at sea. We should also thank Rick Knurr for analytical support. This work was supported through NSF Grants OCE-0221031 and OCE-0351069.

Associate editor: Jeffrey C. Alt

References

Anderson, G.M., Burnham, C.W., 1967. Reactions of quartz and corundum with aqueous chloride and hydroxide solutions at high temperatures and pressures. *Am. J. Sci.* **265**, 12–27.

Anderson, G.M., Burnham, C.W., 1983. Feldspar solubility and the transport of aluminum under metamorphic conditions. *Am. J. Sci.* **283-A**, 283–297.

Berndt, M.E., Person, M.E., Seyfried Jr., W.E., 2001. Phase separation and two-phase flow in seafloor hydrothermal systems: geophysical modeling in the NaCl–H_2O system. Eleventh Annual V.M. Goldschmidt Conference. Geochemical Society, Hot Springs, Va.

Berndt, M.E., Seal II, R.R., Shanks III, W.C., Seyfried Jr., W.E., 1996. Hydrogen isotope systematics of phase separation in submarine hydrothermal systems: experimental calibration and theoretical models. *Geochim. Cosmochim. Acta* **60**, 1595–1604.

Berndt, M.E., Seyfried Jr., W.E., 1997. Calibration of Br/Cl fractionation during subcritical phase separation of seawater; possible halite at 9 to 10°N East Pacific Rise. *Geochim. Cosmochim. Acta* **61**, 2849–2854.

Bischoff, J.L., 1991. Densities of liquids and vapors in boiling NaCl–H_2O solutions; a PVTx summary from 300° to 500 °C. *Am. J. Sci.* **291**, 309–338.

Bischoff, J.L., Rosenbauer, R.J., 1985. An empirical equation of state for hydrothermal seawater (3.2% NaCl). *Am. J. Sci.* **285**, 725–763.

Bischoff, J.L., Rosenbauer, R.J., 1989. Salinity variations in submarine hydrothermal systems by layered double-diffusive convection. *J. Geol.* **97**, 613–623.

Butterfield, D.A., McDuff, R.E., Mottl, M.J., Lilley, M.D., Lupton, J.E., Massoth, G.J., 1994. Gradients in the composition of hydrothermal fluids from the Endeavour segment vent field: phase separation and brine loss. *J. Geophys. Res.* **99**, 9561–9583.

Campbell, A.C., Palmer, M.R., Klinkhammer, G.P., Bowers, T.S., Edmond, J.M., Lawrence, J.R., Casey, J.F., Thompson, G., Humphris, S., Rona, P., Karson, J.A., 1988. Chemistry of hot springs on the Mid-Atlantic Ridge. *Nature* **335**, 514–519.

Carbotte, S., McDonald, K.C., 1992. East Pacific Rise 8–11°30′N: evolution of ridge segments and discontinuities from SeaMarc II and three-dimensional magnetic studies. *J. Geophys. Res.* **97**, 6959–6982.

Chandra, A., 2000. Static dielectric constant of aqueous electrolyte solutions: Is there any dynamic contributions? *J. Chem. Phys.* **113**, 903–905.

Chen, C.-T.A., Marshall, W.L., 1982. Amorphous silica solubilities; IV, behaviour in pure water and aqueous sodium chloride, sodium sulfate, magnesium chloride, and magnesium sulfate solutions up to 350 °C. *Geochim. Cosmochim. Acta* **46**, 279–287.

Cook, D.R., Weisberg, S., 1999. *Applied Regression Including Computing and Graphics*. Wiley-Interscience.

Davies, C.W., 1962. *Ion Association*. Butterworths, London.

Detrick, R.S., Buhl, B., Vera, E., Mutter, J., Orcutt, J., Madsen, J., Brocher, T., 1987. Multi-channel seismic imaging of a crustal magma chamber along the East Pacific Rise. *Nature* **326**, 35–41.

Ding, K., Seyfried Jr., W.E., 1992. Determination of Fe–Cl complexing in the low pressure supercritical region (NaCl fluid): iron solubility constraints on pH of subseafloor hydrothermal fluids. *Geochim. Cosmochim. Acta* **56**, 3681–3692.

Dove, P.M., 1999. The dissolution kinetics of quartz in aqueous mixed cation solutions. *Geochim. Cosmochim. Acta* **63**, 3715–3727.

Dove, P.M., Crerar, D.A., 1990. Kinetics of quartz dissolution in electrolyte solutions using a hydrothermal mixed flow reactor. *Geochim. Cosmochim. Acta* **54**, 955–969.

Dove, P.M., Nix, C.J., 1997. The influence of the alkaline earth cations, magnesium, calcium, and barium on the dissolution kinetics of quartz. *Geochim. Cosmochim. Acta* **61**, 3329–3340.

Edmond, J.M., Measures, C., McDuff, R.E., Chan, L.H., Collier, R., Grant, B., Gordon, L.I., Corliss, J.B., 1979. Ridge crest hydrothermal activity and the balances of the major and minor elements in the ocean: the Galapagos data. *Earth Planet. Sci. Lett.* **46**, 1–18.

Fontaine, F.J., Wilcock, W.S., 2006. Dynamics and storage of brine in mid-ocean ridge hydrothermal systems. *J. Geophys. Res.* **111**. doi:10.1029/2005JB003866.

Fornari, D.J., Shank, T., Von Damm, K.L., Gregg, T.K.P., Lilley, M., Levai, G., Bray, A., Haymon, R.M., Perfit, M.R., Lutz, R., 1998. Time-series temperature measurements at high-temperature hydrothermal vents, East Pacific Rise 9°49′–51′N: evidence for monitoring a crustal cracking event. *Earth Planet. Sci. Lett.* **160**, 419–431.

Fornari, D.J., Tivey, M., Schouten, H., Yoerger, D., Bradley, A., Perfit, M.R., Scheirer, D., Johnson, P., Von Damm, K., Haymon, R., Edwards, M.H., 2004. Submarine lava flow emplacement processes: implications for fluid circulation in the upper ocean crust. In: German, C.R., Lin, J., Parson, L.M. (Eds.), AGU Monograph; Thermal Structure of the Oceanic Crust and Dynamics of Hydrothermal Circulation.

Fournier, R.O., 1983. A method of calculating quartz solubilities in aqueous sodium chloride solutions. *Geochim. Cosmochim. Acta* **47**, 579–586.

Fournier, R.O., Potter, P.W., 1983. An equation correlating the solubility of quartz in water from 25° to 900 °C at pressures up to 10,000bars. *Geochim. Cosmochim. Acta* **46**, 1969–1973.

Fournier, R.O., Rosenbauer, R.J., Bischoff, J.L., 1982. The solubility of quartz in aqueous sodium chloride solution at 350 °C and 180 to 500 bars. *Geochim. Cosmochim. Acta* **46**, 1975–1978.

Ganeyev, I.G., 1975. Solubility and crystallization of silica in chloride. *Dokl. Akad. Nauk* **224**, 248–250.

Gunnarsson, I., Arnorsson, S., 2000. Amorphous silica solubility and the thermodynamic properties of H_4SiO_4 in the range of 0° to 350 °C at P_{sat}. *Geochim. Cosmochim. Acta* **64**, 2295–2307.

Haar, L., Gallagher, J.S., Kell, G.S., 1984. NBS/NRC steam tables: thermodynamic and transport properties and computer programs for vapor and liquid states of water in SI units.

Haymon, R.M., Fornari, D.J., Von Damm, K.L., Lilley, M.D., Perfit, M.R., Edmond, J.M., Shanks, I.W.C., Lutz, R.A., Grebmeier, J.M., 1993. Volcanic eruption of the mid-ocean ridge along the East Pacific Rise crest at 9°45–52′N: direct submersible observations of seafloor phenomena associated with an eruption event in April, 1991. *Earth Planet. Sci. Lett.* **119**, 85–101.

Helgeson, H.C., Kirkham, D.H., Flowers, G.C., 1981. Theoretical prediction of the thermodynamic behavior of aqueous electrolytes at high pressures and temperatures: IV. Calculation of activity coefficients, osmotic coefficients, and apparent molal and standard and relative partial molal properties to 600 °C and 5 kb. *Am. J. Sci.* **281**, 1249–1516.

Hemley, J.J., Montoya, J.W., Marinenko, J.W., Luce, R.W., 1980. General equilibria in the system Al_2O_3–SiO_2–H_2O and some implications for alteration mineralization processes. *Econ. Geol.* **75**, 210–229.

Ho, P.C., Bianchi, H., Palmer, D.A., Wood, R.H., 2000a. Conductivity of dilute aqueous electrolyte solutions at high temperatures and pressures using a flow cell. *J. Sol. Chem.* **29**, 217–235.

Ho, P.C., Palmer, D.A., Gruszkiewicz, M.S., 2001. Conductivity measurements of dilute aqueous HCl solutions to high temperatures and pressures using a flow-through cell. *J. Phys. Chem. B* **105**, 1260–1266.

Ho, P.C., Palmer, D.A., Mesmer, R.E., 1994. Electrical conductivity measurements of aqueous sodium chloride solutions to 600 °C and 300 MPa. *J. Sol. Chem.* **23**, 997–1018.

Ho, P.C., Palmer, D.A., Wood, R.H., 2000b. Conductivity measurements of dilute aqueous LiOH, NaOH, and KOH solutions to high temperatures and pressures using a flow-through cell. *J. Phys. Chem. B* **104**, 12084–12089.

Jasmund, K., 1958. Thermodynamic behavior of quartz and other forms of silica in pure water at elevated temperatures and pressures with conclusion on their mechanism of solution. *J. Geol.* **66**, 595–596.

Johnson, J.W., Oelkers, E.H., Helgeson, H.C., 1992. SUPCRT92—A software package for calculating the standard molal thermodynamic properties of minerals, gases, aqueous species, and reactions from 1-bar to 5000-bar and 0 °C to 1000 °C. *Comput. Geosci.* **18**, 899–947.

Kent, G.M., Harding, A., Orcutt, J.A., 1993. Distribution of magma beneath the East Pacific Rise between the Clipperton Transform and the 9°17′N deval from forward modeling of common depth point data. *J. Geophys. Res.* **98**, 13945–13969.

Khitarov, N.I., 1956. The 400 °C isotherm for the system H_2O–SiO_2. *Am. J. Sci.* **260**, 501–521.

Kitahara, S., 1960. The solubility of quartz in water at high temperatures and high pressures. *Rev. Phys. Chem. Jpn.* **30**, 109–114.

Marshall, W.L., Warakomski, J.M., 1980. Amorphous silica solubilities—II. Effect of aqueous salt solutions at 25 °C. *Geochim. Cosmochim. Acta* **44**, 915–924.

McNabb, A., Fenner, J., 1985. Thermohaline convection beneath the ocean floor CSIRO/DSIR Seminar on convective flows in porous media, Dept. of Sci. and Ind. Res. Wellington, New Zealand.

Mosebach, R., 1957. Thermodynamic behavior of quartz and other forms of silica in pure water at elevated temperatures and pressures with conclusions on their mechanism of solution. *J. Geol.* **65**, 347–363.

Newton, R., Manning, C.E., 2000. Quartz solubility in H_2O–NaCl and H_2–CO_2 solutions at deep crust-upper mantle pressures and temperatures:2–15 kbar and 500 °C–900 °C. *Geochim. Cosmochim. Acta* **64**, 2993–3005.

Oosting, S.E., Von Damm, K.L., 1996. Bromide/chloride fractionation in seafloor hydrothermal fluids from 9–10° N East Pacific Rise. *Earth Planet. Sci. Lett.* **144**, 133–145.

Rubin, K.H., Macdougall, J.D., Perfit, M.R., 1994. $^{210}Po/^{210}Pb$ dating of recent volcanic eruptions on the sea floor. *Nature* **368**, 841–844.

Saccocia, P.J., Seyfried Jr., W.E., 1990. Talc-quartz equilibria and the stability of magnesium chloride complexes in NaCl–$MgCl_2$ solutions at 300, 350, and 400 °C, 500 bars. *Geochim. Cosmochim. Acta* **54**, 3283–3295.

Seewald, J.S., Doherty, K.W., Hammar, T.R., Liberatore, S.P., 2002. A new gas-tight isobaric sampler for hydrothermal fluids. *Deep Sea Res. Part I Oceanogr. Res. Pap.* **49**, 189–196.

Sengers, J.M.H.L., Kamgar-Parsi, B., Balfour, F.W., Sengers, J.V., 1983. Thermodynamic properties of steam in the critical region. *J. Phys. Chem. Ref. Data* **12**, 1–28.

Seward, T.M., 1974. Determination of the first ionization constant of silic acid from quartz solubility in borate buffer solutions to 350 °C. *Geochim. Cosmochim. Acta* **38**, 1651–1664.

Seyfried Jr., W.E., Ding, K., 1993. The effect of redox on the relative solubilities of copper and iron in chlorine-bearing aqueous fluids at elevated temperatures and pressures: an experimental study with application to sub-seafloor hydrothermal systems. *Geochim. Cosmochim. Acta* **57**, 1905–1917.

Seyfried Jr., W.E., Seewald, J.S., Berndt, M.E., Ding, K., Foustoukos, D.I., 2003. Chemistry of hydrothermal vent fluids from the Main Endeavour Field, Northern Juan de Fuca Ridge: Geochemical controls in the aftermath of June 1999 seismic events. *J. Geophys. Res.* **108**, 2429.

Seyfried, W.E.J., Janecky, D.R., Berndt, M.E., 1987. Rocking autoclaves for hydrothermal experiments: II. The flexible reaction-cell system. In: Barnes, H., Ulmer, G. (Eds.), *Hydrothermal Experimental Techniques*. Wiley-Interscience, New York.

Shmulovich, K., Graham, C., Yardley, B., 2001. Quartz, albite and diopside solubilities in H_2O–NaCl and H_2O–CO_2 fluids at 0.5–0.9 GPa. *Contrib. Mineral. Petrol.* **141**, 95–108.

Shock, E.L., Sassani, D.C., Willis, M., Sverjensky, D.A., 1997. Inorganic species in geologic fluids: correlations among standard molal thermodynamic properties of aqueous ions and hydroxide complexes. *Geochim. Cosmochim. Acta* **61**, 907–950.

Sohn, R.A., Fornari, D.J., Von Damm, K.L., Hildebrand, J.A., Webb, S.C., 1998. Seismic and hydrothermal evidence for a cracking event on the East Pacific Rise crest at 9°50′N. *Nature* **396**, 159–161.

Sverjensky, D.A., Shock, E.L., Helgeson, H.C., 1997. Prediction of the thermodynamic properties of aqueous metal complexes to 1000 °C and 5 kb. *Geochim. Cosmochim. Acta* **61**, 1359–1412.

Tierney, L., 1989. XLISP-STAT: a statistical environment based on the XLISP language (Version 2.0). School of Statistics, University of Minnesota, Minneapolis.

Von Damm, K.L., 2000. Chemistry of hydrothermal vent fluids from 9°–10°N, East Pacific Rise; "time zero," the immediate posteruptive period. *J. Geophys. Res.* **105**, 11203–11222.

Von Damm, K.L., 2004. Evolution of the hydrothermal system at East Pacific Rise 9°50′N: geochemical evidence for changes in the upper oceanic crust. In: German, C.R., Lin, J., Parson, L.M. (Eds.), *Mid-Ocean Ridges: Hydrothermal Interactions Between the Lithosphere and Oceans, Geophys. Monogr. Ser*. AGU, Washington, D.C.

Von Damm, K.L., Bischoff, J.L., Rosenbauer, R.J., 1991. Quartz solubility in hydrothermal seawater: an experimental study and equation describing quartz solubility for up to 0.5 M NaCl solutions. *Am. J. Sci.* **291**, 977–1007.

Von Damm, K.L., Buttermore, L.G., Oosting, S.E., Bray, A.M., Fornari, D.J., Lilley, M.D., Shanks III, W.C., 1997. Direct observation of the evolution of a seafloor 'black smoker' from vapor to brine. *Earth Planet. Sci. Lett.* **149**, 101–111.

Von Damm, K.L., Edmond, J.M., Grant, B., Measures, C.I., Walden, B., Weiss, R.F., 1985. Chemistry of submarine hydrothermal solutions at 21°N, East Pacific Rise. *Geochim. Cosmochim. Acta* **49**, 2197–2220.

Von Damm, K.L., Oosting, S.E., Kozlowski, R., Buttermore, L.G., Colodner, D.C., Edmonds, H.N., Edmond, J.M., Grebmeier, J.M., 1995. Evolution of East Pacific Rise hydrothermal vent fluids following a volcanic eruption. *Nature* **375**, 47–50.

Walther, J.V., 1997. Experimental determination and interpretation of the solubility of corundum in H_2O between 350 and 600 °C from 0.5 to 2.2 kbar. *Geochim. Cosmochim. Acta* **61**, 4955–4964.

Walther, J.V., Helgeson, H.C., 1977. Calculation of the thermodynamic properties of aqueous silica and the solubility of quartz and its polymorphs at high pressures and temperatures. *Am. J. Sci.* **277**, 1315–1351.

Wasserburg, G.J., 1958. The solubility of quartz in supercritical water as a function of pressure. *J. Geol.* **66**, 559–578.

Wasserburg, G.J., Wood, J.A.J., 1958. The solubility of quartz at high temperatures and pressures. *Am. J. Sci.*, 438.

Wilcock, W.S., 2004. Physical response of mid-ocean ridge hydrothermal systems to local earthquakes. *Geochem. Geophys. Geosyst.* **5**, Q11009.

Wood, J.A.J., 1958. The solubility of quartz in water at high temperatures and pressures. *Am. J. Sci.* **256**, 40–47.

Xie, Z., Walther, J.V., 1993. Quartz solubilities in NaCl solutions with and without wollastonite at elevated temperatures and pressures. *Geochim. Cosmochim. Acta* **57**, 1947–1955.

Zotov, N., Keppler, H., 2000. In-situ Raman spectra of dissolved silica species in aqueous fluids to 900 °C and 14 kbar. *Am. Mineral.* **85**, 600–604.